AIAA JOURNAL
Vol. 36, No. 8, August 1998

Simulations of Planar Flapping Jets in Confined Channels

Francine Battaglia,* Anil K. Kulkarni,† Jinzhang Feng,‡ and Charles L. Merkle§
Pennsylvania State University, University Park, Pennsylvania 16802

Computational analyses are used to provide a more complete understanding of the mechanisms that contribute to the development of oscillating planar jets. The geometry considered is a two-dimensional jet exhausting into a blind channel, whose open end is opposite to the initial direction such that the jet must turn through 180 deg to exit. The resulting flowfields exhibit three distinct characters that depend on the channel expansion ratio and the Reynolds number. At low Reynolds numbers the flow is steady and symmetric. A symmetry-breaking bifurcation at intermediate Reynolds numbers produces steady asymmetric flows. A Hopf bifurcation at higher Reynolds numbers yields unsteady flows. Predicted critical Reynolds numbers and oscillation frequencies are presented for different expansion ratios. Solutions are obtained from the time-dependent Navier–Stokes equations by means of an incompressible formulation based on dual-time stepping via artificial compressibility.

I. Introduction

LAMINAR flows in two-dimensional symmetrically expanding channels produce either symmetric or asymmetric flowfields.[1–7] The jet flow produced by a sudden expansion remains symmetrically placed in the channel at low Reynolds numbers, but becomes asymmetric at higher Reynolds numbers and attaches to either the upper or lower wall. The steady-state solution that distinguishes these symmetric and asymmetric characteristics is commonly referred to as a symmetry-breaking bifurcation. Experimental investigations of the bifurcation include the work of Durst et al.,[1] Cherdron et al.,[2] and Ouwa et al.[3] Combined numerical–experimental studies were reported by Fearn et al.[4] and Durst et al.,[5] and Shapira et al.[6] used a linear stability analysis. In addition, the authors of this paper investigated the flowfields and bifurcation structure using two independent techniques, numerical simulations and bifurcation calculations, and subsequently compared the results to published work.[7]

The axisymmetric analog of a jet encountering a sudden expansion differs considerably from the planar configuration. The cylindrical channel offers no preferred location to which the jet can attach and remain stationary. Instead, it appears that a round jet will precess about the axis in an unsteady swirl-like fashion, as reported by Nathan and Luxton[8] and Hill et al.[9] Thus, whereas planar jets bifurcate to steady asymmetric solutions, round jets appear to bifurcate to unsteady asymmetric solutions. Although round jets are of interest to us, the dimensionality of the problem is two higher than that of the planar jet, i.e., three spatial dimensions and time vs two spatial dimensions. The literature, however, contains some two-dimensional geometries that have the unsteady character of the suddenly expanded round jet. These unsteady planar flows are not as well characterized as the steady-state flows resulting from a symmetry-breaking bifurcation. In the present paper, studies of a blind channel geometry inspired by existing experimental results are investigated. The information gained from this problem is interesting in its own right while providing insight into the more CPU-intensive three-dimensional unsteady problem.

Received June 20, 1997; revision received April 3, 1998; accepted for publication April 11, 1998. Copyright © 1998 by the American Institute of Aeronautics and Astronautics, Inc. All rights reserved.

*Postdoctoral Research Associate, Department of Mechanical Engineering; currently Postdoctoral Research Associate, Building and Fire Research Laboratory, National Institute of Standards and Technology, Gaithersburg, MD 20899. Member AIAA.

†Professor, Department of Mechanical Engineering.

‡Senior Research Associate, Department of Mechanical Engineering. Member AIAA.

§Professor, Department of Mechanical Engineering; currently Professor, Department of Mechanical Engineering, University of Tennessee Space Institute, Tullahoma, TN 37388. Member AIAA.

The remainder of the paper is laid out as follows. A brief literary survey is presented on the geometric characteristics that have produced unsteady flows. The results show that some sort of flow feedback mechanism is generally required if oscillations are to be observed. The numerical formulation for the unsteady incompressible Navier–Stokes equations is presented in the next section. Results of the numerical simulations are then discussed, beginning with a description of the transitions that lead to multiple flow regimes. Characteristic features of two bifurcations are described, with emphasis on the detailed flowfield for an unsteady flapping jet. Parametric studies of the confined channel flows are also presented for various Reynolds numbers and expansion ratios to ascertain their effects on the critical Reynolds numbers and the frequency of flapping.

As a means of identifying channel geometries that potentially will lead to unsteady oscillations in a planar configuration, we first review findings for laminar flow in symmetrically expanding channels. Some evidence of time-dependent behavior in suddenly expanded flows (in channels with an open downstream end) has been reported by Cherdron et al.,[2] Fearn et al.,[4] Durst et al.,[5] and Sobey and Drazin.[10] These references discuss the possible existence of a Hopf bifurcation that leads to unsteady flows at large Reynolds numbers, but the findings are not conclusive. For example, the unsteady oscillations observed by Cherdron et al.[2] were later determined to have arisen from three-dimensional effects.[5] Similarly, Fearn et al.[4] attempted to find a Hopf bifurcation for symmetrically expanding channels, but found no evidence of one, and also suggested that three-dimensional effects initiated the time-dependent flows. Sobey and Drazin[10] calculated Hopf bifurcations, but their results are for smooth channel expansions that are periodic in the longitudinal direction.

A primary area in which unsteady planar jets have been observed is in the field of fluidics. The channel geometries that have been used for fluidics varied widely, but in general, configurations are such that a jet is discharged from a small channel into a larger one. One key feature of these fluidic oscillations is the presence of some type of feedback mechanism that allows downstream conditions in the jet to be communicated back upstream. A representative geometry is shown in Fig. 1a in which a special passage permits part of the flow to loop back and re-enter the main stream. A related study of fluidic oscillators by Shakouchi[11] revealed that a rectangular jet would produce an oscillating flowfield.

Experiments with symmetrically expanded jets in closed channels in which the jet must turn 180 deg and exit upstream have also been observed to generate oscillating flows for a narrow range of geometries. The geometry of a confined jet, which forms the basis of the configuration studied here, is shown schematically in Fig. 1b and has generated some interesting flows analogous to the open-ended symmetric expansions. Sallam et al.[12,13] reported that the blind configuration led to both symmetric and asymmetric flows, as well as an oscillating jet regime. In the oscillating region, they

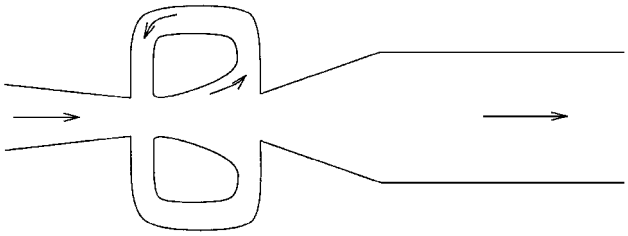

a) Feedback loop

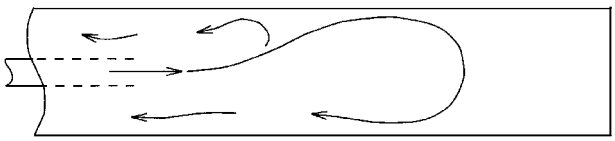

b) Dead end

Fig. 1 Schematic of planar jet expanding into symmetric channel.

found a linear relationship between the frequency of the oscillation and the jet velocity.

One significant finding of both the planar[12,13] and precessing[9] flow experiments that is helpful in our study, is that the absolute location of the closed end has little effect on the unsteady flow. The dead end must be sufficiently far removed from the jet exit to enable a large-scale vortex to form. A stagnant buffer region then fills the remainder of the channel between the vortex and the blind end. The stagnant region effectively masks the location of the blind end and desensitizes the effect of its exact location. This result is exploited in our study to reduce the number of variables by one.

To obtain a geometry that provides an unsteady flapping solution, we have combined the feedback mechanism that is present in the complex geometries used for fluidic oscillators with the blind channel geometry just discussed. The blind channel configuration appears to provide oscillating flows more readily than does the open-ended configuration, whereas the presence of a feedback loop should provide a more regular controlled oscillation.

To date there have been no detailed analytical studies of these intriguing unsteady flowfields. In the present paper, we use the experimental concepts just described to define a simple geometry analogous to the symmetric channel configurations, but with a feedback loop that is an integral part of the flowfield. We then use this geometry along with numerical methods to investigate the dynamics of this class of flows.

II. Problem Formulation

The blind channel geometry chosen for the computations is shown in Fig. 2a. The channel configuration has many features that are analogous to the previous experiments[11–13] but provides a more generic flow domain that includes a simpler and more straightforward feedback mechanism. A smaller channel of height d is positioned inside a larger channel of height D. The flow is introduced at the left end of the inner channel with a parabolic velocity profile. The jet traverses the inner channel and emerges from the right end, expands, and flows toward the blind end of the outer channel. Upon approaching the downstream end wall, the flow turns 180 deg, traverses either the top or bottom (or both) passage(s) between the inner and outer channels, and finally exits at the leftmost opening of width H. The two passages merge before the flow reaches the exit, thereby introducing a communication between the two legs ensuring that a feedback loop is created.

The exit is constrained by including symmetrically placed partial walls at the leftmost end such that $H < D$ (Ref. 14). Allowing $H = D$ encourages the flow to attach to one side of the channel, invariably resulting in inflow on the other side. The partial walls at the exit plane ensure that the reversed flow separates from both the top and bottom walls before exiting so that flow through opening H is always outward (to the left). In turn, meaningful boundary conditions can be enforced. Overall, the geometry provides a flowfield with the desired steady and unsteady jet characteristics and qualitatively simulates experimental results.[11–13]

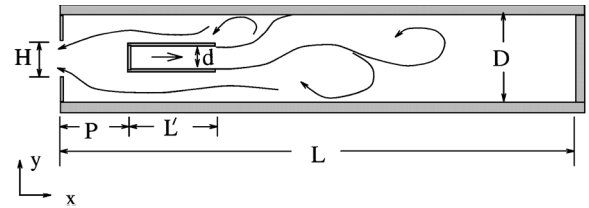

a) Schematic of asymmetric jet in symmetric confined channel

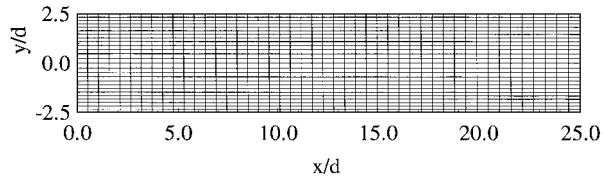

b) Rectangular 141 × 111 grid showing every third node in x and fourth node in y

Fig. 2 Geometrical description of planar jet exhausting into blind channel.

Characteristic parameters of the flow are the channel expansion ratio D/d, the nondimensional exit height H/d, and the Reynolds number $Re = Q'/\nu$, where Q' is the volume flux per unit depth perpendicular to the x–y plane. The lengths of the inner and outer channels, L' and L, respectively, and their relative placement denoted by P in Fig. 2a, complete the formulation. The channel length L was chosen such that the first vortical structure develops completely. The flow then stagnates prior to the blind end and ensures that the actual location has minimal effect on the upstream flow, and length L becomes an insensitive parameter to the flowfield.

III. Numerical Formulation

The incompressible Navier–Stokes equations in generalized coordinates (ξ, η) can be expressed in conservative vector form as

$$\Gamma \frac{\partial \boldsymbol{Q}}{\partial t} + \frac{\partial}{\partial \xi}(\boldsymbol{E} - \boldsymbol{E}_v) + \frac{\partial}{\partial \eta}(\boldsymbol{F} - \boldsymbol{F}_v) = 0 \tag{1}$$

where

$$\Gamma = \begin{pmatrix} 0 & 0 & 0 \\ 0 & 1 & 0 \\ 0 & 0 & 1 \end{pmatrix}, \qquad \boldsymbol{Q} = \frac{1}{J}\begin{pmatrix} p \\ u \\ v \end{pmatrix}$$

$$\boldsymbol{E} = \begin{pmatrix} U \\ uU + py_\eta \\ vU - px_\eta \end{pmatrix}, \qquad \boldsymbol{F} = \begin{pmatrix} V \\ uV - py_\xi \\ vV + px_\xi \end{pmatrix}$$

and

$$\boldsymbol{E}_v = \frac{\nu}{J}\left[(\nabla\xi \cdot \nabla\xi)\frac{\partial(J\boldsymbol{Q})}{\partial \xi} + (\nabla\xi \cdot \nabla\eta)\frac{\partial(J\boldsymbol{Q})}{\partial \eta}\right]$$

$$\boldsymbol{F}_v = \frac{\nu}{J}\left[(\nabla\xi \cdot \nabla\eta)\frac{\partial(J\boldsymbol{Q})}{\partial \xi} + (\nabla\eta \cdot \nabla\eta)\frac{\partial(J\boldsymbol{Q})}{\partial \eta}\right]$$

with the contravariant velocities $U = uy_\eta - vx_\eta$ and $V = vx_\xi - uy_\xi$. The subscripts refer to partial derivatives, and p, u, and v are the primitive variables.

Equation (1) can be converted to the artificial compressibility formulation[15] by changing the physical time t to a pseudotime τ and replacing the matrix Γ with the matrix Γ_p

$$\Gamma_p = \begin{pmatrix} 1/\beta & 0 & 0 \\ 0 & 1 & 0 \\ 0 & 0 & 1 \end{pmatrix}$$

where β is the artificial compressibility parameter. The Euler portion of Eq. (1) becomes fully hyperbolic so that time-marching schemes can be used for either the Euler or the Navier–Stokes equations. The

matrix Γ_p, however, implies that the equations are no longer physically correct for transients, but they regain meaning in the steady-state limit. Time accuracy can be recovered by combining the artificial compressibility method with a dual-time stepping scheme in which the pseudotime derivative $\Gamma_p \partial \boldsymbol{Q}/\partial \tau$ is added to the physical time derivative already appearing in Eq. (1). The real-time solution is then obtained by iterating in pseudotime until $\partial \boldsymbol{Q}/\partial \tau \to 0$.

In the present studies, both steady and unsteady flows were calculated. For both cases, a four-stage Runge–Kutta explicit scheme was used to integrate the solution in pseudotime. The time-accurate cases were formulated by expressing the physical time derivative as a second-order three-point difference. Central differences were used for all spatial derivatives. A complete description of the formulation is given in Ref. 14.

IV. Discussion of Results

The initial results are for an expansion ratio of $D/d = 5$, with an exit height of $H/d = 2$, and channel lengths $L/d = 25$, $L'/d = 5$, and $P/d = 2.5$. A rectangular grid with mild clustering near the walls was used, as shown in Fig. 2b. Numerical tests were performed to determine the grid size needed to resolve the flowfield and generate grid-independent solutions for the present study, as discussed in Ref. 7. The mesh comprised 141×111 grid points with a typical average aspect ratio $\Delta y/\Delta x = 0.25$. The convergence criterion for steady-state calculations was that the relative difference in the residuals between successive iterations be smaller than 10^{-12}. For transient calculations, the relative difference in the residuals between the inner iterations was smaller than 10^{-8}.

A. Steady-State Solutions

Numerical simulations show the confined channel geometry allows symmetric steady solutions, asymmetric steady solutions, and unsteady (flapping) solutions. Results for symmetric and asymmetric steady flows are given in Figs. 3a and 3b, respectively. The symmetric results in Fig. 3a correspond to a Reynolds number (based on the average velocity in the inner channel and the inner channel height) of 25 and show identical small recirculation zones above and below the jet exit (identified by the streamlines). The asymmetric results (Fig. 3b) correspond to $Re = 60$. Here, the recirculation zones are much larger and clearly asymmetric. The flow primarily exits through the lower portion of the duct. Mirror-image solutions with the flow exiting through the upper passage are also easily obtained. In both symmetric and asymmetric cases, the velocities near the rightmost end are negligible.

A sequence of calculations at various Reynolds numbers indicated that these two families of solutions were separated by a symmetry-breaking bifurcation at a critical Reynolds number Re_{c1}. Successive computations of both symmetric and asymmetric solutions with an ever-decreasing Reynolds number range indicated that the flow underwent transition for $25 < Re_{c1} < 30$ for the $D/d = 5$ case. Calculations of Reynolds numbers up to 25 produced stable symmetric solutions, whereas calculations for Reynolds numbers between 30 and 60 produced stable asymmetric solutions. Steady flowfields, however, could no longer be obtained above a Reynolds number of 60, suggesting the presence of a second critical Reynolds number Re_{c2}.

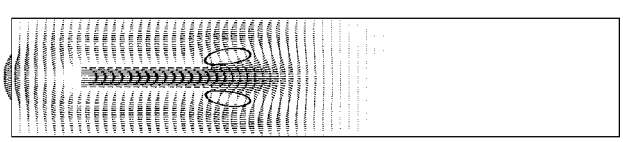

a) Symmetric jet, $Re = 25$, and $D/d = 5$ (streamline contours identify symmetric recirculation patterns)

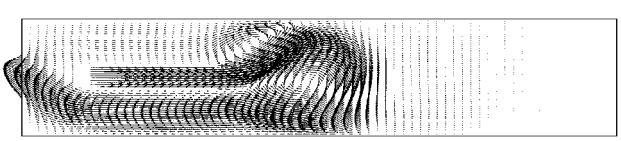

b) Asymmetric jet, $Re = 60$, and $D/d = 5$

Fig. 3 Velocity vectors indicating character of steady-state solutions.

B. Unsteady Solutions

To obtain results beyond these steady solutions, we switched to the time-accurate algorithm. Here, a sequence of computations bracketed the transition between $60 < Re_{c2} < 65$. For Reynolds numbers greater than 65, the flow became unsteady and exhibited a periodic motion. At these supercritical Reynolds numbers, the jet was observed to oscillate between the upper and lower channel walls in a cyclic fashion. The amplitude did not decay with time, and the frequency of the unsteady motion remained constant. This periodic time-dependent character is consistent with a Hopf bifurcation.[16]

C. Physical Features of Transient Flows

A sequence of plots is presented in Fig. 4 showing the velocity vectors in the entire computational domain for eight equally spaced time intervals throughout a representative period of the flapping motion for the case $Re = 100$ and $D/d = 5$. Beginning with the plot at the upper left corner ($t = 0.70$ s), the jet is observed to curve sharply downward as it exits from the inner channel until it almost touches the bottom wall of the outer channel. The outflow moves to the left through the passages both above and below the inner channel, with perhaps slightly more flow going through the upper passage.

Between the initial frame and the next ($t = 0.76$ s), the jet hits the bottom wall and rebounds. The close proximity of the jet with the bottom wall prevents flow through the lower passage so that the entire exit flow is diverted through the upper passage. A large vortex allows some leftward-moving flow in the lower passage, but it is entrained by the rightward-flowing jet such that there is no net mass flux through the lower passage.

In the third frame ($t = 0.82$ s), the jet has moved approximately half-way back to the centerline, and the beginnings of flow between the jet and the bottom wall can be observed, but again it results in a recirculation region rather than a net mass flux through the lower passage. The upper passage continues to be the conduit through which the flow exits. By the fourth frame ($t = 0.88$ s), the jet has moved to approximately the middle of the channel. There is stronger evidence of leftward-moving fluid in the lower passage, yet the upper passage contains nearly all of the exiting mass flux.

The velocity vectors in the fifth frame ($t = 0.94$ s) show the jet is now deflected sharply upward as it exits the inner channel, and a significant mass flow through the lower passage is again observed. The upper passage also continues to transport substantial mass flow, but it can be seen that the jet is about to block this passage. Comparison with the flow at time $t = 0.70$ s shows the present flowfield is nearly a mirror image of the initial frame. Thus, the flow has passed through nearly a one-half period by this point in time.

Moving through the sixth and seventh frames, the jet reflects off the top wall, terminates flow through the upper passage, and exits through the lower passage. The jet continues to move downward until it has nearly reached the centerline ($t = 1.12$ s). The next succeeding frame, $t = 1.18$ s, would nearly duplicate the flow configuration seen in the first frame ($t = 0.70$ s). Consequently, the periodic variation of the flapping motion has been traced through one cycle with a period of motion approximately 0.48 s.

To demonstrate the stationary nature of the oscillatory flow, the time history of the instantaneous pressure and the streamwise and cross-stream components of the velocity at two points in the flowfield are shown in Figs. 5 and 6. These results verify that the oscillation remains stationary without growth or decay. The results of Fig. 5 are on the centerline ($y/d = 0$), whereas those of Fig. 6 correspond to conditions near the top wall (y/d near 2.5). Both sampling points correspond to the approximate streamwise location $x_p/d = 2.68$, at which the jet impacts the wall (where x_p is measured from the inner channel exit). The flapping frequency as determined from these results is approximately 2.0 Hz, corresponding to a Strouhal number of 0.19 based on the average velocity through the outer channel and channel height D.

Further inspection of the results in Fig. 5 confirms that the streamwise velocity u is always positive and reaches a maximum every time the jet passes through the centerline. There are two peaks in the streamwise velocity during each complete cycle of the flapping

jet, and the frequency of the u velocity is twice that of the flapping jet. The pressure also shows two cycles for every complete cycle of the flapping jet. The pressure trace leads the streamwise velocity trace by 90 deg such that the u velocity is a maximum when the pressure passes through zero. The cross-stream velocity has the same period as the jet. As the jet moves upward, the v velocity on the centerline is positive, and when it moves downward, the v velocity is negative. The results in Fig. 5 also show that the cross-stream velocity oscillation is symmetric about $v = 0$.

The time traces for the pressure and velocity components near the top wall in Fig. 6 are generally analogous to the results in Fig. 5. However, the streamwise velocity is primarily negative, indicating the flow at the sampling location is reversed through most of the period. The corresponding v-velocity component is nearly zero throughout the period because of the relative proximity of the wall. Finally, the pressure at this location again exhibits two peaks per cycle, but the first amplitude is only one-third that of the second. Thus, the frequency of the pressure has dropped to match that of the flapping jet, although there remains a remnant of the dual frequency noted on the centerline. The u velocity at this near-wall region also exhibits the same frequency as the jet.

The results of Fig. 6 show that the pressure at the near-wall point reaches a maximum at $t = 0.45, 0.96$, and 1.47 s. Detailed inspection of the flowfield at $t = 0.96$ s shows the peak in pressure corresponds to the time when the jet impacts the wall. Note that Fig. 6 also indicates that the streamwise velocity u at this position is nearly zero at $t = 0.96$, another indication that the jet is stagnating on the wall. Thus, the pressure is a maximum, and the velocities at the wall vanish when the jet impacts.

Figure 7 shows the streamwise variations of the pressure along the top wall at six different times during one-half of the jet flapping cycle. As time progresses, maximum and minimum pressure peaks occur. The peaks increase in magnitude as the jet moves closer to the wall, with the largest pressure peak at $x_p/d = 2.68$ and $t = 0.96$ s. The maximum pressure during the cycle corresponds to the instant at which the jet impacts the wall.

The cross-stream variation of the pressure at $x_p/d = 2.68$ is shown in Fig. 8 for the same six time intervals during the half-cycle of the flapping jet. Again, the maximum peak occurs at $t = 0.96$ s and corresponds to the results in Fig. 7. In addition, Fig. 8 shows that the pressure on the opposite side of the channel ($y/d < 0$) is considerably lower throughout this half of the cycle. Of course, the opposite wall experiences higher pressures during the second-half of the jet-flapping cycle when the jet is in the lower half of the channel.

Inspection of the flowfields in the unsteady regime shows that only minor details of the overall flow patterns are modified as the Reynolds number is increased. This can been seen from the instantaneous velocity vector fields for $Re = 100$, 500, and 1000 in Fig. 9. The velocities in each plot have been nondimensionalized by their respective mean velocities. For each Reynolds number condition, the results are shown at the time when the jet just touches the upper wall so that nearly the same phase of the oscillation is compared. In each case, a single dominant vortical structure is present just beyond the inner channel exit. At higher Reynolds numbers there is evidence of an increased number of smaller eddies that shed from the jet and interact in the flow exiting through the passages. The solutions also show that the jet bends more severely toward the wall as the Reynolds number increases. By and large, the solutions are qualitatively similar.

D. Mapping the Flow Bifurcations

The confined channel simulations indicate that three different stable flow regimes exist: 1) steady symmetric flow, 2) steady asymmetric flow (with two possible solutions), and 3) unsteady, periodic flow. The three regimes can be found parametrically by varying the Reynolds number and are distinguished from each other by a pair of transition points. The first transition is a symmetry-breaking bifurcation Re_{c1} that separates the symmetric flow solutions at low Reynolds numbers from the asymmetric solutions at intermediate Reynolds numbers. The second transition (that gives rise to a flapping jet region) is a Hopf bifurcation Re_{c2} that separates the intermediate Reynolds number asymmetric solutions from the unsteady solutions at higher Reynolds numbers.

The three flow regimes and the approximate location of the transition points that separate them are presented in Fig. 10 for a channel expansion ratio of five. The results in Fig. 10 show the maximum cross-stream velocity (normalized by the mean velocity in channel d) on the channel centerline for all Reynolds number solutions between 10 and 1000. Symmetric flow, for which the cross-stream velocity is zero along the entire centerline, exists up to a Reynolds number of 25. This is shown as the horizontal line at $v = 0$. For Reynolds numbers between 30 and 60, two asymmetric solutions exist. The solution with positive v velocity corresponds to flow attached to the upper wall whereas negative v velocity implies attachment to the lower wall. The solid lines used to identify the symmetric and asymmetric solutions in these first two regimes clearly show the symmetry-breaking bifurcation. As noted in Sec. IV.A, computational procedures only allow the critical Reynolds number to be bracketed to within a finite tolerance.

The dashed lines in Fig. 10 represent the unsteady periodic solutions. These results show the peak-to-peak amplitude of the cross-stream velocity on the centerline at the point where it is a maximum. Thus, the two dashed lines do not represent distinct solution branches, but rather the envelope inside which the solution oscillates during a single period. It is interesting that the envelope of the unsteady solution is a more or less continuous extrapolation of the maximum velocities observed in the adjacent asymmetric flow regime. Again, the transition region is bracketed to within a finite band lying between $Re = 60$ and $Re = 65$.

Shown in Table 1 are the results for expansion ratios five and seven. (For $D/d = 7$, the channel dimensions are $L/d = 25$, $L'/d = 7$, and $P/d = 3.5$.) As can be seen, increasing the expansion ratio decreases both critical Reynolds numbers. The trend that is observed here for both the symmetry-breaking and the Hopf bifurcations is consistent with the trends for the symmetry-breaking bifurcations cited in Refs. 1–7. The overall trends emphasize that flow instabilities arise at lower Reynolds numbers as the expansion ratio is increased.

To quantify the turning point of the jet as it expands from the inner channel, the location of the maximum pressure point at the wall, the position where the jet stagnates, was compared for each case. A summary of the data is presented in Table 1 for the nondimensional distance x_p/d downstream of the inner channel exit. The results show that increasing the Reynolds number for a fixed expansion ratio moves the maximum pressure location successively closer to the inner channel exit. For an expansion ratio of five, the maximum pressure location moves 0.72 channel heights toward the exit plane as the Reynolds number is increased from 100 to 1000. A similar trend with Reynolds number is observed for the larger expansion ratio case, except that the larger outer channel causes the jet to impact the wall somewhat farther downstream. The results suggest that the unsteady effects become "stronger" as the Reynolds number is increased. The jet is bent at larger and larger angles and flaps more violently.

E. Characterization of Flapping Frequency

A final important analysis of the flapping regime is a characterization of its Strouhal number. A plot showing the manner in which frequency varies with Reynolds number and expansion ratio is given

Table 1 Comparisons of critical Reynolds numbers and reattachment locations for varying Reynolds numbers and expansion ratios for planar confined flows

D/d	Critical Reynolds number	Reynolds number	x_p/d
5	$25 < Re_{c1} < 30$	100	2.68
	$60 < Re_{c2} < 65$	500	2.32
		750	2.32
		1000	1.96
7	$20 < Re_{c1} < 25$	100	3.50
	$40 < Re_{c2} < 45$	500	3.25
		750	3.00
		1000	2.25

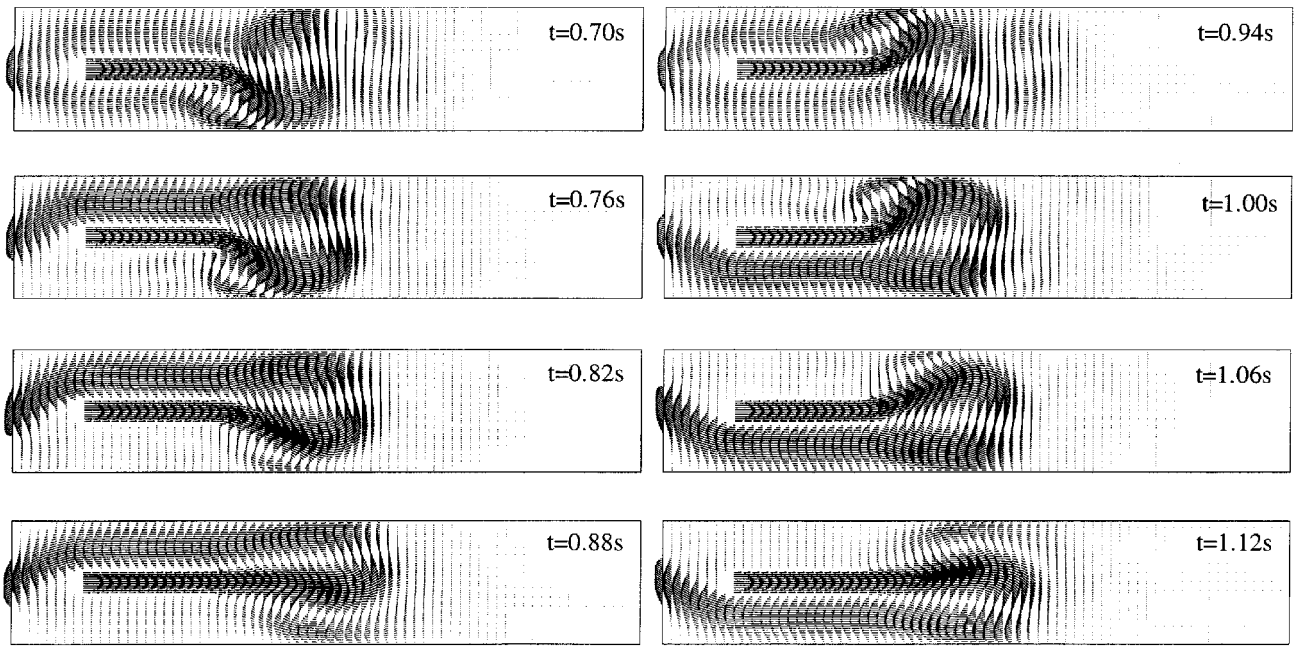

Fig. 4 Velocity vectors of transient solution of unsteady asymmetric jet for $Re = 100$ and $D/d = 5$.

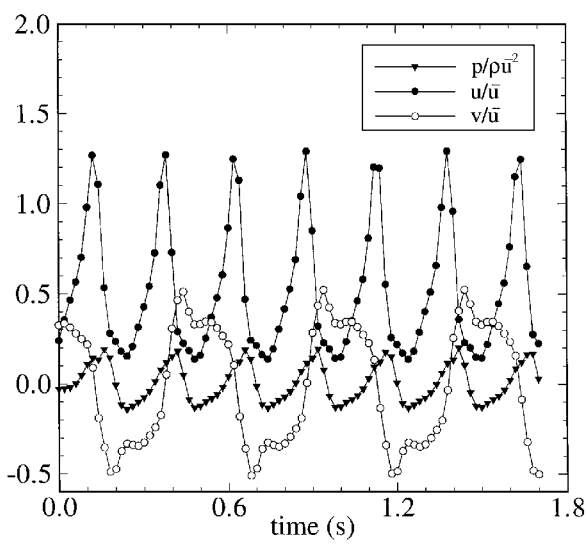

Fig. 5 Nondimensionalized variables vs time at $x_p/d = 2.68$ and $y/d = 0.0$ for $Re = 100$ and $D/d = 5$.

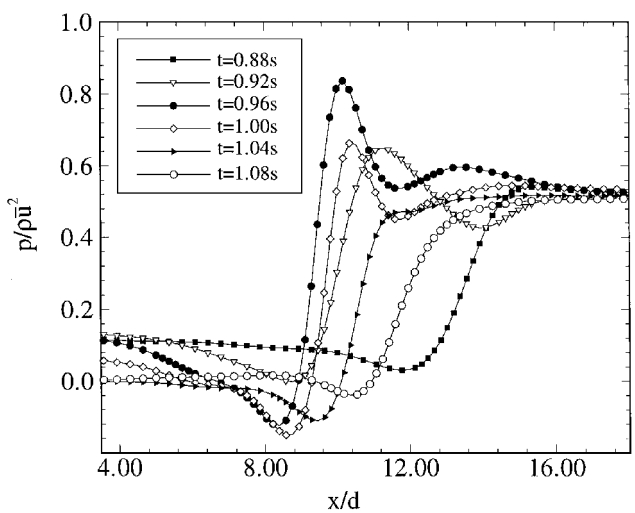

Fig. 7 Pressure distribution vs streamwise position at $y/d = 2.5$ for $Re = 100$ and $D/d = 5$.

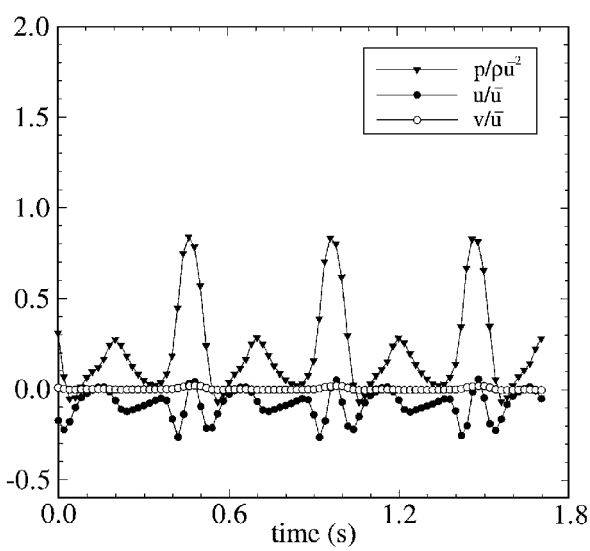

Fig. 6 Nondimensionalized variables vs time at $x_p/d = 2.68$ and $y/d = 2.46$ for $Re = 100$ and $D/d = 5$.

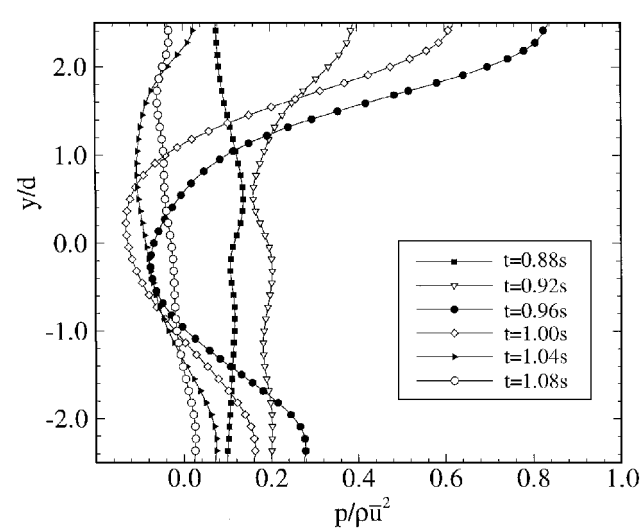

Fig. 8 Cross-stream position vs pressure distribution at $x_p/d = 2.68$ for $Re = 100$ and $D/d = 5$.

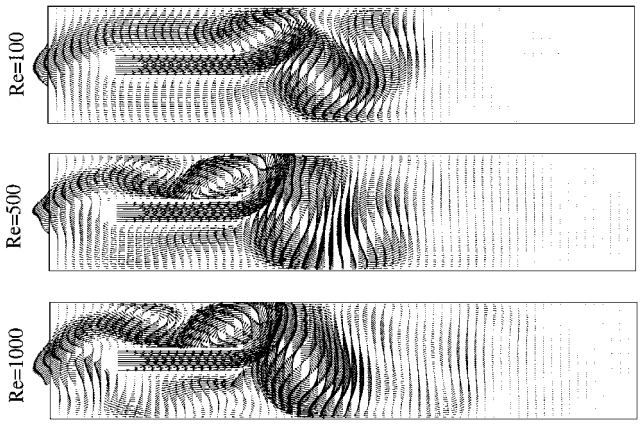

Fig. 9 Nondimensional velocity vectors of flow in confined channel at *Re* = 100, 500, and 1000 for *D/d* = 5.

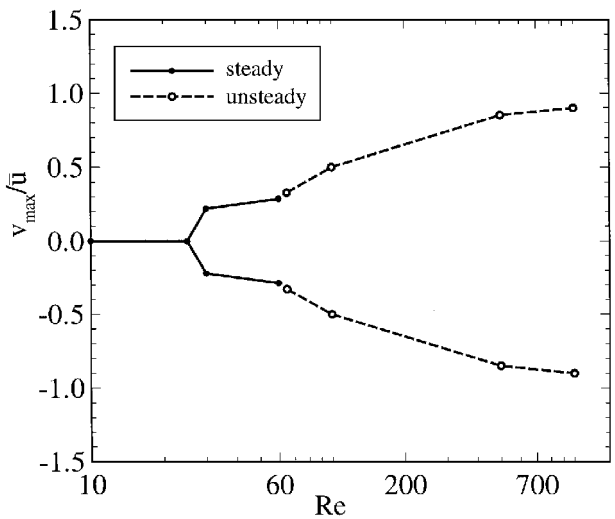

Fig. 10 Numerical simulations of regimes corresponding to symmetry-breaking and Hopf bifurcations for expansion ratio *D/d* = 5.

in Fig. 11. The results for expansion ratio $D/d = 5$ indicate the frequency increases almost linearly with Reynolds number, whereas for the larger expansion ratio a weak nonlinear behavior is observed. The nonlinear increase in frequency is probably the result of degrading grid resolution for the case of $D/d = 7$ and $Re = 1000$. The results should, however, remain qualitatively valid.

The Strouhal number used to describe the motion can be defined in many ways. Here, we have chosen to use $Sr_D = f\,D/\bar{u}_D$, where $\bar{u}_D$ is the average velocity in the outer channel, D. Results based on this Strouhal number are on the order of 0.3 (see Fig. 11). The Strouhal numbers for an expansion ratio of five are constant with Reynolds number except for the lowest value, which is slightly less than the other three values. The Strouhal numbers for expansion ratio $D/d = 7$ gradually drift upward with Reynolds number reflecting the weak nonlinearity in the frequency-Reynolds number curve.

An alternative Strouhal number based on the average velocity and height of the inner channel has also been considered, but differs from Sr_D by the square of the expansion ratio (D/d), and gives Strouhal numbers of order 0.01. The present definition of Strouhal number Sr_D is consistent with the one used by Hill et al.[9] (based on momentum flux) and brings the Strouhal numbers for both geometrical configurations into close proximity. The experimental findings of Sallam et al.[12,13] also indicate a linear relationship between frequency and Reynolds number. Their experiments were for channel expansion ratios $D/d = 6.25$ and 7.5 with domain lengths $3.0 \le (L - L')/d \le 5.6$. The results of a nondimensional frequency based on the average velocity and height of the outer channel gives Strouhal numbers for a range of 0.047–0.285, which is in reasonable qualitative agreement with the results presented here. Note, however, that the results of Sallam et al.[12,13] were for high Reynolds number flows with shorter domain lengths.

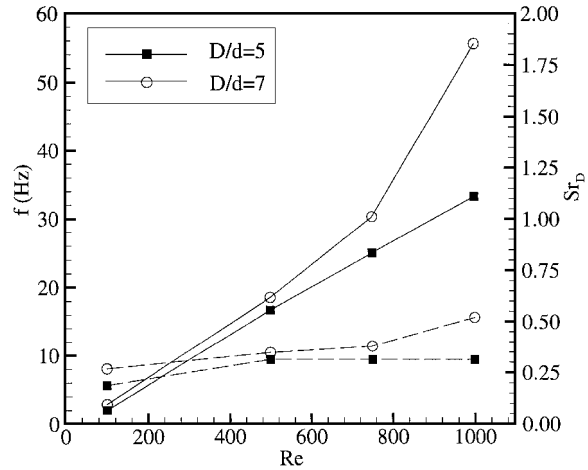

Fig. 11 Relationship between Reynolds number with frequency (——) and Strouhal number (– – –) for fixed expansion ratios.

V. Conclusions

Numerical simulations have been used to assess the characteristic flow features of a two-dimensional jet expanding into a symmetric blind channel. The results show the presence of two bifurcations that lead to multiple flow regimes. The first transition is a symmetry-breaking bifurcation to an asymmetric steady solution, whereas the second transition is a Hopf bifurcation to an unsteady solution. The symmetry-breaking bifurcation is analogous to the symmetric-asymmetric transition observed in earlier work on sudden expansions. The unsteady solutions appear to be introduced through an internal feedback loop inside the flow domain. At Reynolds numbers above the critical value for the Hopf bifurcation, the jet flaps back and forth between the channel walls.

The characteristics of the flowfield depend on the Reynolds number and the expansion ratio. The onset of the symmetry-breaking and Hopf bifurcations occurs at lower Reynolds numbers when the expansion ratio is increased. The frequency of oscillation associated with the flapping increases linearly with the Reynolds number such that the Strouhal number is nearly constant. Proper choice of the nondimensionalizing parameters gives a Strouhal number that is only weakly dependent on the expansion ratio. The flow patterns of the transient motion are nearly independent of Reynolds number except for the rate of flapping. Finally, the results indicate that the peak-to-peak velocity envelope inside which the unsteady flapping solution oscillates is qualitatively similar to the magnitudes of the cross-stream velocity for the asymmetric steady solutions.

Acknowledgment

The authors would like to thank the Center for Academic Computing at the Pennsylvania State University for the computing time made available on the IBM RS/6000 SP.

References

[1] Durst, F., Melling, A., and Whitelaw, J. H., "Low Reynolds Number Flow over a Plane Symmetric Sudden Expansion," *Journal of Fluid Mechanics*, Vol. 64, No. 1, 1974, pp. 111–128.

[2] Cherdron, W., Durst, F., and Whitelaw, J. H., "Asymmetric Flows and Instabilities in Symmetric Ducts with Sudden Expansions," *Journal of Fluid Mechanics*, Vol. 84, No. 1, 1978, pp. 13–31.

[3] Ouwa, Y., Watanabe, M., and Asawo, H., "Flow Visualization of a Two-Dimensional Water Jet in a Rectangular Channel," *Japanese Journal of Applied Physics*, Vol. 20, No. 1, 1981, pp. 243–247.

[4] Fearn, R. M., Mullin, T., and Cliffe, K. A., "Nonlinear Flow Phenomena in a Symmetric Sudden Expansion," *Journal of Fluid Mechanics*, Vol. 211, Feb. 1990, pp. 595–608.

[5] Durst, F., Pereira, J. C. F., and Tropea, C., "The Plane Symmetric Sudden-Expansion Flow at Low Reynolds Numbers," *Journal of Fluid Mechanics*, Vol. 248, 1993, pp. 567–581.

[6] Shapira, M., Degani, D., and Weihs, D., "Stability and Existence of Multiple Solutions for Viscous Flow in Suddenly Enlarged Channels," *Computers and Fluids*, Vol. 18, No. 3, 1990, pp. 239–258.

[7] Battaglia, F., Tavener, S. J., Kulkarni, A. K., and Merkle, C. L., "Bifurcation of Low Reynolds Number Flows in Symmetric Channels," *AIAA Journal*, Vol. 35, No. 1, 1997, pp. 99–105.

[8]Nathan, G. J., and Luxton, R. E., "Mixing Enhancement by a Self-Exciting, Asymmetric Precessing Flow-Field," *Transport Phenomena in Heat and Mass Transfer*, edited by J. A. Reizes, Vol. 2, Elsevier, London, 1992, pp. 1297–1307.

[9]Hill, S. J., Nathan, G. J., and Luxton, R. E., "Precession in Axisymmetric Confined Jets," *Twelfth Australasian Fluid Mechanics Conference* (Sydney, Australia), R. W. Bilger, Univ. of Sydney, Sydney, Australia, 1995, pp. 1–4.

[10]Sobey, I. J., and Drazin, P. G., "Bifurcations of Two-Dimensional Channel Flows," *Journal of Fluid Mechanics*, Vol. 171, 1986, pp. 263–287.

[11]Shakouchi, T., "A New Fluidic Oscillator, Flowmeter, Without Control Port and Feedback Loop," *Journal of Dynamic Systems, Measurement and Control*, Vol. 111, No. 3, 1989, pp. 535–539.

[12]Sallam, T. M., Kaji, M., Nakanishi, S., Ishigai, S., and Matsumoto, S., "Characteristics of Reversed Flow Due to Jet Issuing to Dead-End Channel," Osaka Univ., TR 1539, Osaka, Japan, 1980, pp. 217–224.

[13]Sallam, T. M., Kaji, M., Nakanishi, S., and Ishigai, "Visualization of Recirculating Flows in Reversed-Flow Furnace Models," *Flow Visualization II*, edited by W. Merzkirch, Hemisphere, New York, 1982, pp. 57–61.

[14]Battaglia, F., "Numerical Simulations of Instabilities and Asymmetric Characteristics of Suddenly Expanded Channel Flows," Ph.D. Thesis, Dept. of Mechanical Engineering, Pennsylvania State Univ., University Park, PA, May 1997.

[15]Chorin, A., "A Numerical Method for Solving Incompressible Viscous Flow Problems," *Journal of Computational Physics*, Vol. 2, 1967, pp. 12–26.

[16]Glendinning, P., *Stability, Instability and Chaos: An Introduction to the Theory of Nonlinear Differential Equations*, Cambridge Texts in Applied Mathematics, Cambrige Univ. Press, New York, 1994, Chap. 3.

K. Kailasanath
Associate Editor